Low-temperature resistivity of $La_{0.7}Sr_{0.3}MnO_3$ ultra thin films: Role of quantum interference effects

L. Maritato,* C. Adamo, C. Barone, G. M. De Luca, A. Galdi, P. Orgiani, and A. Yu. Petrov

Dipartimento di Fisica "E.R. Caianiello," Università di Salerno and CNR-INFM Salerno, 84081, Baronissi (SA), Italy

(Received 18 November 2005; revised manuscript received 21 February 2006; published 31 March 2006)

The low-temperature (<60 K) transport properties of as-grown $La_{0.7}Sr_{0.3}MnO_3$ ultrathin films, deposited by the molecular beam epitaxy, have been investigated as a function of the sample thickness (from 40 to 3.5 nm) and in the presence of an external magnetic field. With decreasing thickness, a clear low-temperature resistivity minimum slightly affected by the application of the magnetic field has been observed, and its presence has been possibly interpreted in terms of quantum interference effects. As a function of the thickness, a crossover from a three-dimensional (3D) to a two-dimensional (2D) behavior of the system takes place below 20 nm. A re-entrant 3D behavior is induced in ultrathin films by the application of large (>20 kOe) magnetic fields. Negative values of the magnetoresistance have been observed in all of the investigated samples for all of the measured magnetic fields.

DOI: 10.1103/PhysRevB.73.094456 PACS number(s): 75.47.Gk, 72.15.Gd, 73.50.Jt

I. INTRODUCTION

In the recent years, several works have pointed out the possible presence of quantum interference effects (QIE) in the low-temperature magnetotransport properties of colossal magnetoresistance (CMR) manganites.[1–9] In particular, the appearance of a low-temperature (<40 K) resistivity minimum has been tentatively interpreted as the sign of temperature-dependent quantum corrections driven by Coulomb interactions in the transport properties of the ferromagnetic state of bulk, single crystal, and thin film manganites. The transport properties of any material are strongly dependent on its form (single crystalline, polycrystalline) and studies on polycrystalline and single-crystalline CMR manganite samples[6] have shown that the application of an external magnetic field reduces or suppresses the minimum for ceramic samples while rendering it even more pronounced in single crystals. These differences in the magnetic field dependence of the resistivity minimum have been traced back to different main conduction mechanisms, spin-polarized tunneling through grain boundaries in ceramic samples,[10] QIE in single crystals. On the other hand, as shown for $La_{0.8}Sr_{0.2}MnO_3$ large grain ceramic samples,[6] the resistivity upturn is present in a magnetic field as large as 13.6 T, indicating the simultaneous presence of both the above-mentioned conduction mechanisms. Therefore, even though QIE seem to play an important role in the appearance of this low-temperature resistivity upturn, other effects are thought to be simultaneously at work and to influence especially the magnetoresistive behavior.

The QIE influence the transport properties via two different sources:[11] (i) electron-electron interactions enhanced by a strong disorder potential, and (ii) weak localization due to the finite dimensions of the system. The total resistivity in the first order corrections is given by[9]

$$\rho(H,T) = \rho_0 + \rho_m(H,T) - \rho_0^2[\sigma_{ee}(H,T) + \sigma_{wl}(H,T)], \quad (1)$$

where ρ_0 is the residual resistivity, $\rho_m(H,T)$ the magnetic resistivity contribution, $\sigma_{ee}(H,T)$ the electron-electron interaction effects corrections, and $\sigma_{wl}(H,T)$ the weak localization contribution.

Even though, in general, the two sources produce effects of the same order of magnitude, it is clear that for bulk and thick film samples, the second term (weak localization) should be of less importance, while in the case of very thin films, it should play an increasing role.

In high quality manganite thin films, in principle, it is possible to study the QIE by varying, in a controlled way, different parameters (stoichiometry, thickness, disorder) which should play important roles in the low-temperature conduction mechanisms. In particular, the control on the thickness of the films allows us to vary the dimensions of the investigated system, opening the possibility to discriminate between Coulomb interactions and weak localization effects and to observe crossovers from three-dimensional (3D) to 2D behaviors.

The available studies on QIE in manganite films are rare[8,9] and the few performed on samples with properties which can be regarded as representatives of bulk material[9] is limited to $La_{0.7}Ca_{0.3}MnO_3$ samples with thickness $t > 100$ nm. A major problem in dealing with ultrathin (thickness below 10 nm) manganite films, is the presence of the so-called dead layer, with depressed conducting and/or magnetic properties at the interface between the film and the substrate.[13] Nevertheless, in all the works performed so far, a low-temperature negative magnetoresistance (MR) has been always observed, while the Coulomb interaction driven QIE should give positive MR.[11] Negative MR can be due to QIE related to weak localization or to the typical CMR manganites behavior. Moreover, the scattering by magnetic impurities and by impurities with spin-orbit coupling has been demonstrated to strongly influence the sign of the MR,[12] rendering even more difficult the disentanglement of the different contributions to QIE in CMR manganites.

By using the molecular beam epitaxy (MBE) deposition technique, we have been able to produce as-grown ultrathin films of $La_{0.7}Sr_{0.3}MnO_3$ with transport and magnetic properties comparable to those of the bulk samples. We have pro-

TABLE I. Characteristic parameters for the investigated samples: the thickness t, the out-of-plane crystallographic c axis, the metal-insulator transition temperature T_{MI}, and the resistivity minimum ρ_{min}.

Sample	t (nm)	c *axis* (nm)	T_{MI} (K)	ρ_{min} (m Ω cm)
LSMO40	40	0.385	357	0.11
LSMO36	36	0.385	380	0.13
LSMO27	27	0.386	368	0.17
LSMO20	20	0.386	354	0.40
LSMO18	18	0.385	341	0.66
LSMO10	10	0.383	350	1.23
LSMO6	6	0.381	359	3.92
LSMO4	3.5	0.379	218	19.6

duced samples with thickness in the range 40–3.5 nm investigating their low-temperature transport properties also in the presence of an external magnetic field up to 70 kOe. With decreasing thickness, the films have shown a clear low-temperature resistivity minimum slightly affected by the application of the magnetic field. The transport properties of the investigated samples have been interpreted in light of QIE. As a function of the thickness, a crossover from a 3D to a 2D behavior of the system takes place below 20 nm. This crossover is observed even more clearly in the presence of an externally applied magnetic field. These results open also the possibility of checking similarities in the low-temperature conduction mechanisms in both the CMR infinite-layer and low dimensional bilayer manganites.[14]

II. EXPERIMENT

The films have been deposited on $SrTiO_3$ (100) single crystal substrates using a MBE codeposition technique in the presence of a mixture of $O_2+5\%O_3$ with pressure $P=2.6\times10^{-4}$ Pa. The typical total deposition rate has been 10^{-2} nm/s. The pressure of the mixture has been held constant also during the post deposition cool down and the film thickness has been varied acting on the deposition process time. More details on the growth procedure are reported elsewhere.[15] The as-grown samples have been structurally characterized by x-ray diffraction. Sharp rocking curves and interference fringes around the reflection in the θ-2θ scans have been measured, showing the high crystallographic quality of the films. Reflectivity measurements have been performed to evaluate the film thickness and the surface roughness. Atomic force microscopy analysis has also been used to check film roughness. Typical film roughness values were in the range 0.5–1.0 nm, comparable with those of the used substrates. The out-of-plane and in-plane lattice sample parameters have been measured as a function of the thickness using symmetrical and asymmetrical reflections, respectively. The out-of-plane crystal lattice values, along with all the other relevant parameters of the investigated samples, are reported in Table I. The in-plane crystal lattice parameters of all the samples have been found to fully match to the in-plane lattice parameter of the substrate. The stoichiometry of the produced samples has been checked out by energy dispersive spectroscopy and rutherford backscattering analysis. Electrical transport measurements have been carried out by standard four-probe dc technique, mechanically pressing at room temperature indium pads onto the film surface. To minimize possible contamination of the samples, no photolithographic processes have been carried out on the as-grown samples, and because manganites are known to have resistance sensitive to the application of high electric field,[16] all the transport measurements shown in this work have been taken in regions of linear current-voltage behavior. The MR properties have been investigated using a Niobium based superconducting solenoid able to reach up to 70 kOe with the applied magnetic field always in the plane of the film. To remove possible effects on MR due to the Lorentz force, the MR was measured with the magnetic field always along to the current direction.

III. TRANSPORT PROPERTIES IN ZERO MAGNETIC FIELD

In Fig. 1(a) are shown the resistivity ratio $\rho/\rho_{\min}$ versus the temperature T curves in the range 4.2–60 K for the investigated samples with a different thickness from 40 to 3.5 nm. $\rho_{\min}$ is defined as the lowest resistivity value and for the sake of clarity each curve is shifted from the other by an offset of 0.2. While for the samples with thicknesses larger than 20 nm the resistivity monotonically decreases with decreasing temperatures, a minimum in the resistivity starts to be increasingly pronounced in the samples with a thickness smaller than or equal to 20 nm. The temperature at which the minimum occurs also depends on the sample thickness, increasing with decreasing thicknesses. As shown in Table I, all the investigated samples have metal-insulator (MI) transition temperatures higher than 340 K, with the only exception of the 3.5 nm thick film. When measured, the obtained Curie temperatures have been always close to the MI temperatures (generally around 10 K smaller).[17] The lowest resistivity values [$\rho(4.2\ \mathrm{K})$ for samples thicker than 20 nm, and $\rho(T\,\mathrm{min})$ for the other samples] range from around 0.1 m Ω cm to around 20 m Ω cm going from the thickest to the thinnest sample, see Table I. The Mott's maximum value for metallic resistivity is around 10 m Ω cm, and it seems, therefore, plausible, in the case of the investigated samples, to interpret the appearance of the resistivity minimum in terms of QIE related to electron-electron interactions enhanced by a strong disorder potential. On the other hand, the weak localization effects should play an increasing role with the decrease of the film thickness affecting the actual dimensionality of the system. From the data in Table I, one can observe that, with the exception of the 3.5 nm thinnest sample, the lowest resistivity value constantly increases of a factor of 3 when halving the thickness, possibly indicating that the main contribution to the resistivity increase is coming from the localization effects and not from the enhanced disorder.

Following Lee and Ramakrishnan,[11] thin film systems are truly 2D for localization effects when L_{Th}, the length scale up to which electrons diffuse without inelastic collisions, is

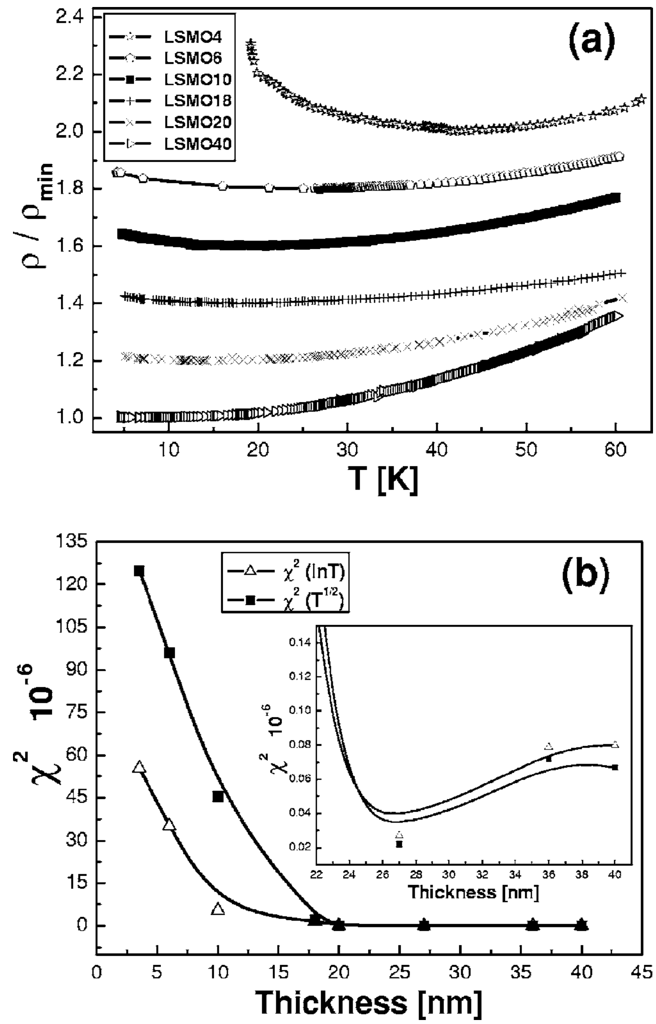

FIG. 1. (a) Temperature dependence of the resistivity ratio $\rho/\rho_{\min}$ for the investigated samples (for the sake of clarity each curve is shifted from the other by an offset of 0.2). (b) Thickness dependence of the calculated normalized χ^2 test related to the two fitting procedures obtained using Eqs. (2) and (3). In the inset to (b), the normalized χ^2 test values as a function of the thickness in the region above 20 nm are shown in detail. The solid lines are guides to the eyes.

larger than the film thickness t. Now, $L_{Th}\sim(L_iL_e)^{1/2}$, with L_i and L_e the inelastic and elastic scattering lengths, respectively, and since the boundary scattering in very thin films is generally the basic elastic scattering mechanism, i.e., $L_e\sim t$, this implies that a thin film is 2D for localization effects when $t<L_i$. On the other hand, with respect to Coulomb interactions, the system is 2D when $t<(\hbar D/kT)^{1/2}$, where D is the diffusion coefficient and k the Boltzmann constant. By using the Einstein relation, we can write $D/kT=\sigma(T)/ne^2$, with n the carrier density at the Fermi energy and $\sigma(T)$ the conductivity at temperature T, to estimate the quantity $(\hbar\sigma_{\min}/ne^2)^{1/2}$. Taking $n=2.4\times10^{22}/\mathrm{cm}^3$ (Ref. 18) and $\sigma_{\min}$ from the data in Fig. 1(a), $(\hbar\sigma_{\min}/ne^2)^{1/2}$ decreases monotonically with the thickness, going from 0.39 nm in the sample 40 nm thick to 0.03 nm for LSMO4. Therefore, for all the investigated sample thicknesses, the system should be 3D with respect to Coulomb interactions.

The dimensionality of the system influences the temperature behavior of the electron-electron interaction σ_{ee} and weak localization σ_{wl} first term corrections to the conductivity. In the 2D case, both the corrections have a logarithmic dependence, while in the 3D case, the electron-electron σ_{ee} term goes as $T^{1/2}$ and the weak localization σ_{wl} correction behaves as $T^{p/2}$, with p a parameter depending on the dominant scattering mechanism, estimated equal to $\frac{3}{2}$ for electron-electron collisions in the dirty limit, 2 for electron-electron scattering in the clean limit and 3 for electron-phonon processes.[11]

In thin film systems, the size of the localization anomalies, probably due to the disorder-induced increase of inelastic decay rates, has been generally found to be surprisingly small, rendering difficult the distinction between weak localization and Coulomb interaction effects. In the manganite thin films investigated so far,[8,9] the large values of the thickness ($\geqslant$100 nm) have further decreased the possibility to observe conductivity corrections due to localization effects. As an example, Kumar *et al.*[8] have successfully fitted the $\rho(T)$ curves showing low-temperature minima in $La_{0.7}Ca_{0.3}MnO_3$ thin films, using the formula

$$\rho(T)=\frac{1}{\sigma_0+BT^{1/2}}+AT^n, \tag{2}$$

with σ_0, B, A, and n free fitting parameters. In Eq. (2), all the scattering processes such as electron-phonon, electron-magnon, and electron-electron are assumed to be adequately described by a single power law (AT^n), and the validity of the Mathiessen's rule is postulated. In the same work,[8] the authors have also tried to fit the experimental data using a logarithmic dependence for the conductivity corrections

$$\rho(T)=\frac{1}{\sigma_0+C\ln T}+AT^n, \tag{3}$$

but have always found a worse agreement in terms of the normalized χ^2 test, with values higher by a factor of 6 when compared to those obtained using Eq. (2).

We have tried to fit our $\rho(T)$ curves using both Eqs. (2) and (3). QIE are expressed in terms of corrections to the conductivity and the validity of Eqs. (2) and (3) is generally restricted to the limit of low temperatures.[11] All the results presented in the following, in terms of the resistivity, yield the same conclusions if carried out analyzing the conductivity.

In Table II, the results of the fitting procedure are reported in terms of the normalized χ^2 test and some of the fitting parameter values. The χ^2 values related to the two fitting procedures are generally of the same order of magnitude, but an interesting behavior is observed as a function of the film thickness. In fact, while at large thicknesses (above 20 nm) the χ^2 values are in the range of 10^{-8} and those associated to the $T^{1/2}$ dependence are always smaller, for small thickness (below 20 nm), the χ^2 values for both the fitting procedures are in the 10^{-6} range (comparable to those obtained by Kumar *et al.*) and those associated with the logarithmic dependence are now smaller, as shown in Fig. 1(b). In the limit of ultrathin films, the difference between the $\chi^2(T^{1/2})$ and the

TABLE II. Normalized χ^2 values and fitting parameters: B $(\mathrm{m}\,\Omega\,\mathrm{cm}\,\mathrm{K}^{1/2})^{-1}$, C $(\mathrm{m}\,\Omega\,\mathrm{cm})^{-1}$, and σ_0 $(\mathrm{m}\,\Omega\,\mathrm{cm})^{-1}$, using both Eqs. (2) and (3), for the investigated samples.

Sample	χ^2 $(T^{1/2})\times 10^{-6}$	χ^2 $(\ln T)\times 10^{-6}$	B	C	σ_0
LSMO40	0.067	0.080	0.139	0.172	13.438
LSMO36	0.072	0.079	0.047	0.057	7.731
LSMO27	0.022	0.027	0.034	0.039	5.916
LSMO20	0.052	0.055	0.035	0.047	2.267
LSMO18	2.108	1.604	0.034	0.040	1.408
LSMO10	45.44	5.446	0.024	0.033	0.726
LSMO6	96.11	35.10	0.0073	0.011	0.228
LSMO4	124.9	55.46	0.014	0.021	0.0192

$\chi^2(\ln T)$ values increases although the absolute values of both the χ^2 point toward the 10^{-5} range. The values of the parameters B, C, and σ_0 are generally decreasing with decreasing thickness, see Table II. In particular, σ_0 goes from values in the range of 10 $(\mathrm{m}\,\Omega\,\mathrm{cm})^{-1}$ for the sample 40 nm thick to values of the order of 100 $(\mu\Omega\,\mathrm{cm})^{-1}$ for the samples with thickness of 6 nm. The values of the parameter B are lower than those obtained by Kumar *et al.*[8] and the parameter n, not reported in Table II, is generally in the range 2–3.[19]

The crossover from a $T^{1/2}$ to a $\ln T$ behavior in the low-temperature resistivity dependence with decreasing thicknesses can be related to a change in the dimensionality of the system, going from 3D for samples thicker than 20 nm to 2D in the limit of ultrathin samples. On the other hand, the absolute differences between the $\chi^2(T^{1/2})$ and the $\chi^2(\ln T)$ values are very small for thicknesses larger than 20 nm, probably indicating the decreasing role played by the QIE correction terms in Eqs. (2) and (3). The comparison between the sample thicknesses and the values of $(\hbar D/kT)^{1/2} = (\hbar\sigma_{min}/ne^2)^{1/2}$ seems to rule out possible dimensionality effects induced by the electron-electron σ_{ee} contribution and could indicate that the crossover is related to the weak localization σ_{wl} term. In this case, the thickness at which the crossover is observed ($\sim$20 nm) has a straight physical interpretation, giving the order of magnitude of the inelastic scattering length L_i, in the investigated temperature range. The temperature dependence of $L_i \sim T^{-p/2}$ can also explain the observed thickness dependence of the T_{min} values. In fact, assuming that the low-temperature resistivity minimum signals the temperature at which the QIE correction terms start to play a major role [i.e., the temperature at which $L_i(T)\sim t$], the thickness dependence of T_{min} should be strictly related to the temperature dependence of the inelastic scattering length L_i. In effects, our experimental results suggest $L_i(T)\sim T^{-n}$, with $n\sim 1.6$, close to the expected value in the case of a dominant scattering mechanism due to electron-phonon interactions. If the weak localization plays a major role in determining the low-temperature resistivity behavior of manganite films, for thicknesses in the 3D regime (above 20 nm) the $\rho(T)$ curves in Fig. 1(a) should be better described using the formula

$$\rho(T) = \frac{1}{\sigma_0 + BT^{p/2}} + AT^n, \tag{4}$$

with p equal to $\frac{3}{2}$, 2, 3, depending on the dominant scattering mechanism.[11] The results of the fitting procedure in terms of the χ^2 test, by using Eq. (4), have always given a worst agreement with respect to those obtained using a $T^{1/2}$ dependence. In particular, the χ^2 values obtained with $p=2,3$ were more than one order of magnitude higher, while those with $p=\frac{3}{2}$ were slightly higher but of the same order of magnitude. We point out that the experimental values of σ_{min} obtained in the ultrathin film limit are generally higher than the Mott's limit, and, therefore, the possible presence of consistent effects due to electron-electron interactions cannot be completely ruled out.

IV. MAGNETIC FIELD TRANSPORT PROPERTIES

The measurements performed in zero magnetic fields indicate that QIE play an important role in the low-temperature conduction mechanisms of manganite ultrathin films, although it is generally difficult to discriminate between the two main QIE contributions, i.e., Coulomb interactions and weak localization. The study of the transport properties of ultrathin manganite films, in the presence of an external magnetic field, can help in disentangling the two terms and determining their relative sizes. Moreover, the presence of an externally applied magnetic field should influence the dimensionality of the system.

In Figs. 2(a) and 2(b) are reported the $\rho(T)$ curves in the same temperature range of Fig. 1(a), taken in different magnetic fields for the samples LSMO10 and LSMO6, respectively. All the curves present a resistivity minimum in which temperature T_{min}, as a function of the applied magnetic field, is plotted in Fig. 3(a). The depth of the minima, defined as $[\rho(4.2K)-\rho(T_{min})]/\rho(4.2K)$, for both the samples is reported in Fig. 3(b). From the data it is clear that the application of a magnetic field does not suppress the presence of the resistivity minimum, ruling out possible effects due to the grain boundaries. Both the samples LSMO10 and LSMO6 have $\rho(T)$ curves in zero magnetic fields well described by a logarithmic dependence, which, as seen in the previous paragraph, is typical of a 2D system. Using Eqs. (2) and (3) we

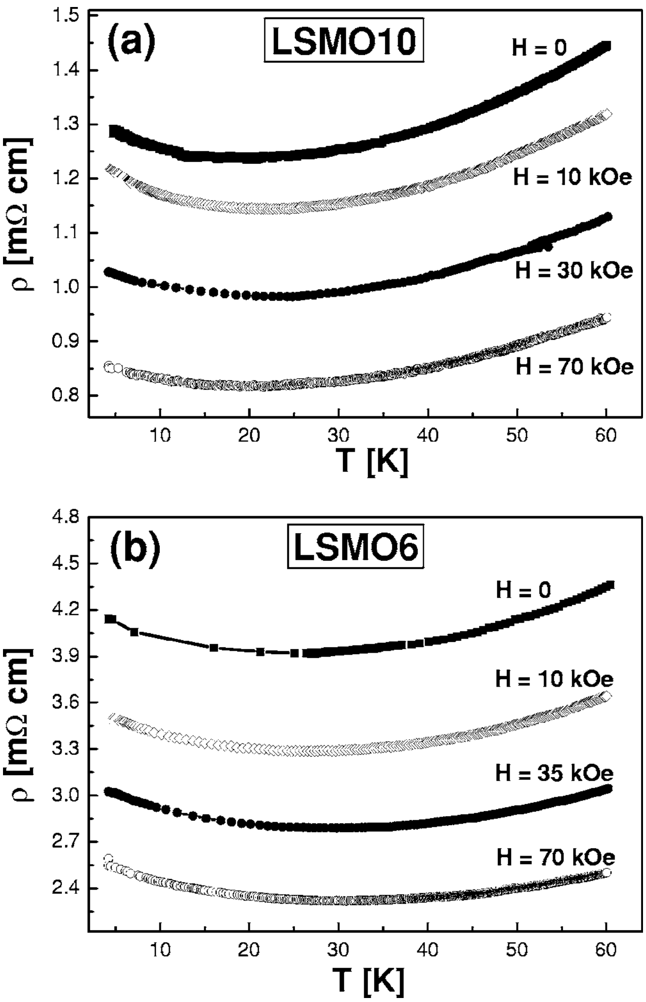

FIG. 2. Resistivity ρ vs T curves, taken at different magnetic fields, for the samples LSMO10 (a) and LSMO6 (b). The solid lines are guides to the eyes.

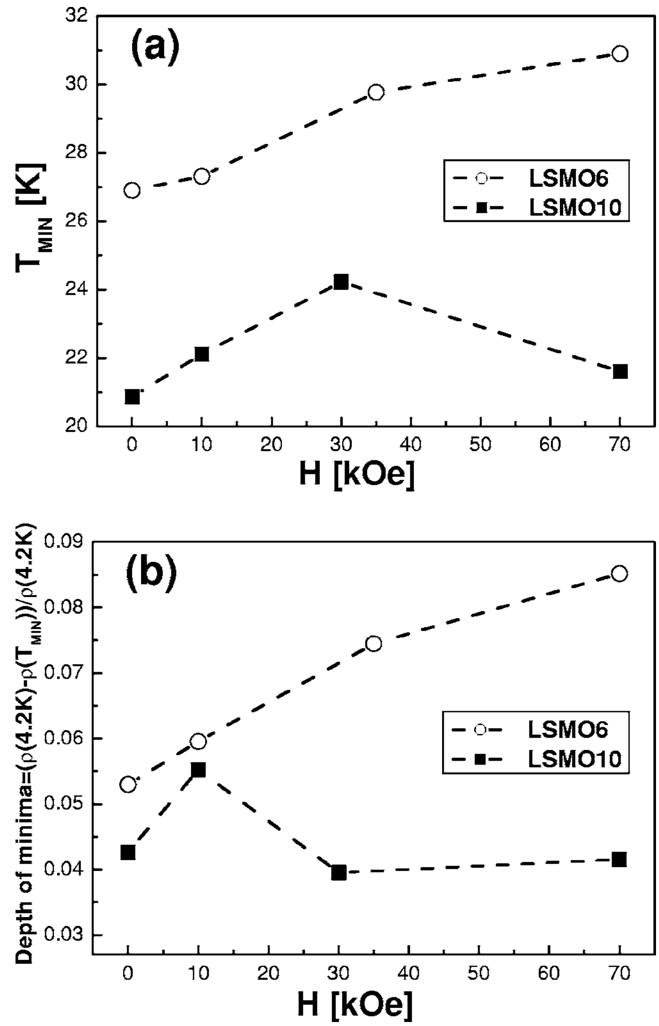

FIG. 3. (a) The temperature associated with the resistivity minimum T_{min} and (b) the depth of the minima versus the magnetic field H, for the samples LSMO6 and LSMO10. The dashed lines are guides to the eyes.

have fitted the experimental curves in Figs. 2(a) and 2(b).

In Table III we have reported the results of the fitting procedures, in terms of the normalized χ^2 test and some of the fitting parameter values as a function of the applied external magnetic field. As for the zero field case, the best χ^2 values are always in the $10^{-5}-10^{-6}$ range. For both the samples investigated, the normalized $\chi^2(T^{1/2})$ and $\chi^2(\ln T)$ test values have different field dependences, as shown in Figs. 4(a) and 4(b). While the $\chi^2(T^{1/2})$ value decreases with increasing field, the $\chi^2(\ln T)$ one increases with the magnetic field, in agreement with the general idea that the application of a magnetic field should play against localization.

In both the samples LSMO10 and LSMO6, a crossover field H_{cross}, around 10 kOe, separates a low field region where the $\chi^2(\ln T)$ is smaller from a high field zone in which it is $\chi^2(T^{1/2})$ which gives the best values. In the high field region where the $\chi^2(T^{1/2})$ is lower, the difference with the $\chi^2(\ln T)$ is larger than one order of magnitude. In terms of the analysis performed in the previous section, in the low field zone the conduction properties of the samples show a 2D behavior, while in the high field region the systems behave as 3D. This dimensional crossover is induced by the external magnetic field. We have tried to compare the observed values of H_{cross} with those expected for several characteristic fields, such as, for example, the one related to weak localization effects, H_l, that originating from the orbital contribution, H_{so}, and the one due to the spin-splitting part of the Coulomb interaction, H_s. Following Ref. 11, we have $H_l \sim (h/2e)L_{th}^{-2}$, with $L_{th}^{-2} \sim L_i L_e$, and assuming, as already done in the previous paragraph, $L_e \sim t$ and taking, from the results of the $\rho(T)$ dependence on the sample thickness, $L_i \sim 20$ nm, we obtain typical H_l values in the range of 100 kOe. The spin-splitting field is defined[11] $H_s \sim kT/g\mu_B$, where k is the Boltzmann constant, g the Landè factor, and μ_B the Bohr magneton. At $T=30$ K, we have $H_s \sim 200$ kOe. Both these fields have typical values much larger than H_{cross}. The H_{so} field is reduced with respect to H_s by the factor $(k_F l)^{-1}$ which, using a free electron estimate for k_F and l, gives $k_F l \sim 100$, and $H_{so} \sim 2$ kOe, about one order of magnitude lower than H_{cross}. On the other hand, the typical values of the crossover field give Landau orbit lengths $L_H = (\hbar/2eH_{cross})^{1/2} \sim 10-20$ nm, very close to the thickness of

TABLE III. Normalized χ^2 values and fitting parameters: B (m Ω cm K$^{1/2}$)$^{-1}$, C (m Ω cm)$^{-1}$, and σ_0 (m Ω cm)$^{-1}$ [Eqs. (2) and (3)], as a function of the applied external magnetic field H (kOe) for the samples LSMO10 and LSMO6.

Sample	H	χ^2 ($T^{1/2}$)$\times 10^{-6}$	χ^2 (ln T)$\cdot 10^{-6}$	B	C	σ_0
LSMO10	0	45.44	5.4465	0.024	0.033	0.726
LSMO10	10	27.27	7.456	0.036	0.044	0.755
LSMO10	30	2.231	19.22	0.029	0.036	0.917
LSMO10	70	1.358	47.47	0.037	0.049	1.095
LSMO6	0	96.11	35.10	0.0073	0.011	0.228
LSMO6	10	73.23	67.34	0.0089	0.012	0.267
LSMO6	35	57.49	92.68	0.0125	0.017	0.304
LSMO6	70	13.52	186.1	0.0164	0.022	0.360

the samples under investigation. One possible explanation of the observed crossover field, could be, therefore, traced back to the comparison between the sample thickness t and the Landau orbit L_H. When it is $t > L_H$, the presence of the film boundaries does not strongly influence the charge carrier motion and the system behaves essentially as 3D, while at $t < L_H$ the film boundaries play an important role resulting in a 2D behavior of the system.

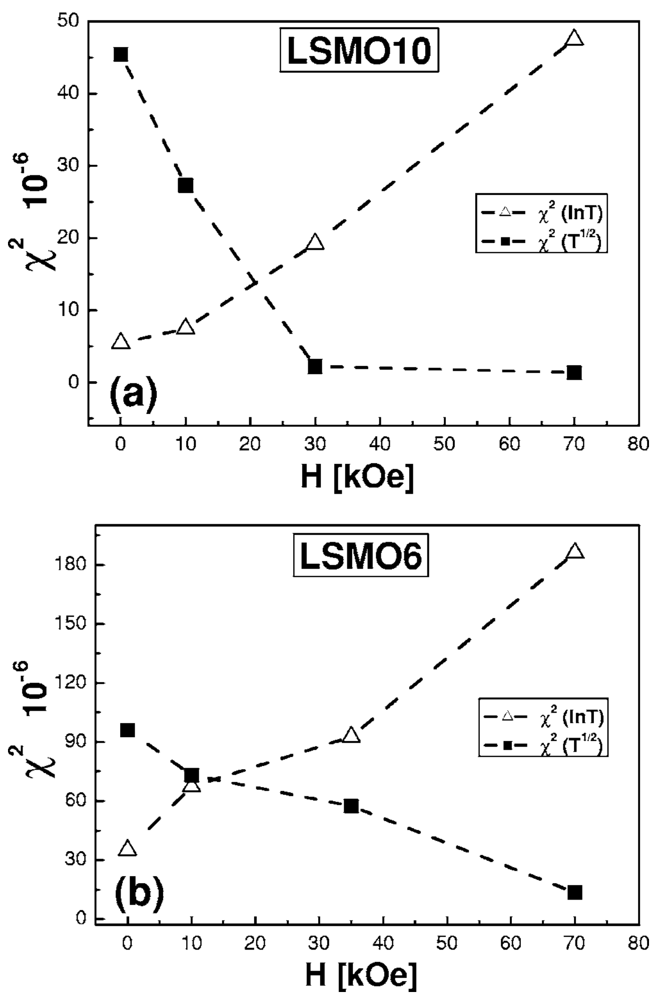

FIG. 4. Magnetic field dependence of the calculated normalized χ^2 test related to the two fitting procedures using Eqs. (2) and (3), for the sample LSMO10 (a) and LSMO6 (b). The dashed lines are guides to the eyes.

In Fig. 5, are shown the MR curves, in a magnetic field of 10 kOe, as a function of the temperature, for the samples LSMO40, LSMO10, and LSMO6. The MR is defined as $[\rho(H,T)-\rho(0,T)]/\rho(0,T)$, and for all the samples has negative values in all the temperature ranges 350 to 4.2 K. In particular, around room temperatures, all the curves present the well-known CMR peak with similar MR values, but at temperatures below 60 K, while the sample LSMO40 has very low MR values, in agreement with the behavior observed in single-crystalline manganites, the samples LSMO10 and LSMO6 have negative MR values more than one order of magnitude larger than those observed for LSMO40, and in the case of LSMO6, even higher than the CMR value measured at room temperature. Such a large low-temperature MR effect seems typical of ultrathin manganite films and cannot be related to bulk behaviors. In the framework of QIE, the Coulomb interaction mechanism should result in a positive MR while the weak localization should produce negative MR effects. In a truly 2D system the MR due to a weak localization is predicted to be negative only

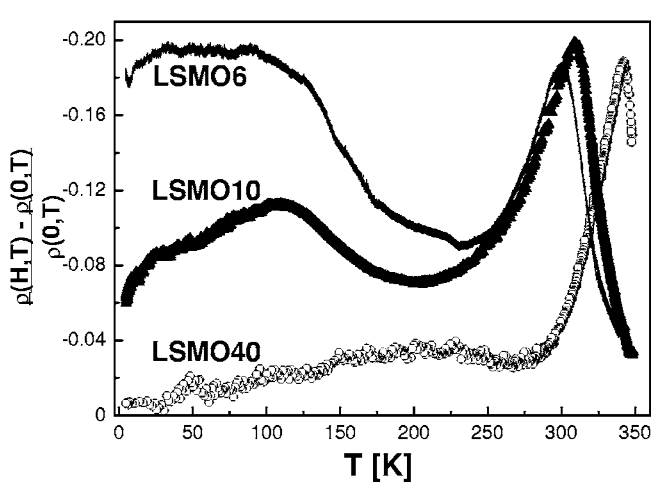

FIG. 5. Magnetoresistance curves, in a magnetic field of 10 kOe, as a function of temperature, for the samples LSMO6, LSMO10, and LSMO40.

when the field is applied perpendicularly to the plane of the system.[11] A negative MR, due to weak localization, is foreseen also for a magnetic field in the plane of the film when the thickness is smaller than the Landau orbit L_H.[20] The observed negative values of MR even in the high field region, where $t > L_H$, can be due, as an example, to a more complex situation in which spin-orbit scattering, Zeeman splitting, and inelastic scattering are simultaneously at work,[21] or to a nontrivial magnetic ordering present in the strained ultrathin films of manganites.[22] More studies to enlighten these aspects are currently in progress.

V. CONCLUSIONS

We have analyzed the low-temperature transport properties of MBE produced ultrathin films of $La_{0.7}Sr_{0.3}MnO_3$, with variable thicknesses and conducting and magnetic properties comparable to those of the bulk samples. The films with thicknesses smaller than 20 nm have shown a clear low-temperature resistivity minimum slightly affected by the application of an in-plane external magnetic field up to 70 kOe. QIE well describe the observed $\rho(T)$ curves with the low-temperature upturn. A 3D-2D crossover in the conducting behavior takes place in the investigated systems as a function of the thickness. Moreover, in ultrathin films, the application of the external magnetic field influences the dimensionality of the conducting mechanisms, inducing a field driven 3D-2D crossover in which possible interpretation can be related to the comparison between the dimensions of the Landau orbits and the thickness of the samples. The negative values of MR observed in all the investigated samples for all the measured magnetic fields point out the need of nontrivial scenarios related to the simultaneous presence of different scattering mechanisms or of complex magnetic orderings to satisfactorily explain the experimental data.

*Electronic address: maritato@sa.infn.it

[1] A. Barman, M. Ghosh, S. Biswas, S. K. De, and S. Chatterjee, Solid State Commun. **106**, 691 (1998).

[2] A. Barman, M. Ghosh, S. Biswas, S. K. De, and S. Chatterjee, J. Phys.: Condens. Matter **10**, 9799 (1998).

[3] A. Tiwari and K. P. Rajeev, Solid State Commun. **111**, 33 (1999).

[4] A. Michalopoulou, E. Syskakis, and C. Papastaikoudis, J. Phys.: Condens. Matter **13**, 11615 (2001).

[5] E. Syskakis, G. Choudalakis, and C. Papastaikoudis, J. Phys.: Condens. Matter **15**, 7735 (2003).

[6] M. Auslender, A. E. Kar'kin, E. Rozemberg, and G. Gorodetski, J. Appl. Phys. **89**, 6639 (2001).

[7] P. Chen, D. Y. Xing, and Y. W. Du, Phys. Rev. B **64**, 104402 (2001).

[8] D. Kumar, J. Sankar, J. Narayan, R. K. Singh, and A. K. Majumdar, Phys. Rev. B **65**, 094407 (2002).

[9] M. Ziese, Phys. Rev. B **68**, 132411 (2003).

[10] E. Rozemberg, M. Auslender, I. Felner, and G. Gorodetski, J. Appl. Phys. **88**, 2578 (2000).

[11] P. A. Lee and T. V. Ramakrishnan, Rev. Mod. Phys. **57**, 287 (1985).

[12] G. Bergmann, Phys. Rev. Lett. **48**, 1046 (1982).

[13] J. Z. Sun, D. W. Abraham, R. A. Rao, and C. B. Eom, Appl. Phys. Lett. **74**, 3017 (1999); A. de Andrs, J. Rubio, G. Castro, S. Taboada, J. L. Martinez, and J. M. Colino, *ibid.* **83**, 713 (2003); M. Angeloni, G. Balestrino, N. G. Boggio, P. G. Medaglia, P. Orgiani, and A. Tebano, J. Appl. Phys. **96**, 6387 (2004).

[14] T. Okuda, T. Kimura, and Y. Tokura, Phys. Rev. B **60**, 3370 (1999); Q. A. Li, K. E. Gray, and J. F. Mitchell, *ibid.* **63**, 024417 (2000); C. L. Zhang, X. J. Chen, C. C. Almasan, J. S. Gardner, and J. L. Sarrao, *ibid.* **65**, 134439 (2002).

[15] A. Yu. Petrov, C. Aruta, S. Mercone, C. Adamo, I. Alessandri, and L. Maritato, Eur. Phys. J. B **40**, 11 (2004).

[16] A. Asamitsu, Y. Tomioka, H. Kuwahara, and Y. Tokura, Nature (London) **388**, 50 (1997); H. Oshima, K. Miyano, Y. Konishi, M. Kawasaki, and Y. Tokura, Appl. Phys. Lett. **75**, 1473 (1999).

[17] P. Orgiani, A. Yu. Petrov, C. Adamo, C. Aruta, C. Barone, G. M. De Luca, A. Galdi, M. Polichetti, D. Zola, and L. Maritato (unpublished).

[18] B. F. Woodfield, M. L. Wilson, and J. M. Byers, Phys. Rev. Lett. **78**, 3201 (1997).

[19] S. Mercone, C. A. Perroni, V. Cataudella, C. Adamo, M. Angeloni, C. Aruta, G. De Filippis, F. Miletto, A. Oropallo, P. Perna, Y. Petrov, U. S. diUccio, and L. Maritato, Phys. Rev. B **71**, 064415 (2005).

[20] B. L. Altshuler, A. G. Aronov, and B. Z. Spivak, JETP Lett. **33**, 94 (1981).

[21] S. Maekawa and H. Fukuyama, J. Phys. Soc. Jpn. **50**, 2516 (1981).

[22] Z. Fang, I. V. Solovyev, and K. Terakura, Phys. Rev. Lett. **84**, 3169 (2000).